Influence of static rotor imbalance on the roller bearing damage due to inverter-induced bearing currents

Martin Weicker, Omid Safdarzadeh, Andreas Binder
Technische Universität Darmstadt
Institute for Electrical Energy Conversion
Landgraf-Georg-Straße 4
64283 Darmstadt, Germany
Tel.: +49 / (0) 6151 16 24191
E-Mail: mweicker@ew.tu-darmstadt.de
URL: http://www.ew.tu-darmstadt.de

Acknowledgements

This IGF Project IGF-Nr. 21488 N (FVA Nr. 650 III) of the Research Association for Drive Technology (FVA) was supported via AiF within the program for promoting the Industrial Collective Research (IGF) of the Federal Ministry of Economic Affairs and Climate Action (BMWK), based on a resolution of the German Parliament. We acknowledge also the support of our industrial partner *SEW Eurodrive*.

Keywords

«bearing currents», «voltage source inverter», «induction motor», «static rotor imbalance»

Abstract

The influence of static rotor imbalance on the generation of bearing fluting due to bearing currents is experimentally investigated. For that six inverter-fed induction machines with the rated power of 1.5 kW and three with the rated power of 11 kW were tested with especially prepared bearings. The machines were operated with three different static rotor imbalances (U0, U1, U2) to test the imbalance influence on the fluting effect due to discharge and rotor-to-ground bearing currents. The damaging effect of inverter-induced bearing currents is influenced by the parameters “rotor speed”, “bearing temperature”, “bearing grease” and “grounding conditions” of the inverter-motor-system. The impact of a static rotor imbalance on the damaging process caused by the parasitic bearing currents is so far unknown. Therefore it shall be clarified, if the combination of static rotor imbalance and bearing currents may damage the bearing raceway surfaces much faster than without imbalance. As a concluding result our test procedures showed no acceleration of bearing deterioration due to static rotor imbalances.

Introduction

High frequency bearing currents may occur due to the common-mode inverter output voltage in inverter-fed AC machines [3]. If the apparent bearing current density surpasses a limit of 0.1 … 0.3 A/mm² the bearing currents may cause damage and thus increased wear to the mechanical roller bearings [3]. This might lead to unexpected early bearing failures, increasing the machine downtime and reducing the bearing lifespan. The four main types of these inverter-induced bearing currents are circulating, electrical discharge machining (EDM), capacitive and rotor-to-ground bearing currents [3]. Parameters that influence the type and magnitude of these bearing currents are rotor speed, radial and axial bearing forces, bearing temperature, viscosity and conductivity of the bearing grease, the resulting electrical impedance of the bearing and the grounding conditions of the inverter-motor-system [3], [4], [6].

Early research on the mechanism of bearing damage due to electrical bearing currents was already done in 1943 [5], focusing on the fluting damage. The initiation mechanism of fluting from starting with craters on the raceway due to “sparking“ in the lubrication film between raceway and roller

elements, leading to vibrations and the raceway fluting pattern, is still not understood in detail. So also recent publications deal with the propagation of fluting at the bearing raceway [2]. The process of generation of the fluting pattern on the bearing raceway surface due to bearing currents is still under research. We investigated, if an additional mechanical vibration may accelerate the fluting process and may damage the bearing surface faster. For that, we investigated the influence of different static rotor imbalances at TEFC standard cage-induction machines with a rated power of 1.5 kW and 11 kW, respectively, in combination with EDM and rotor-to-ground bearing currents, when being operated at voltage source PWM IGBT inverters.

Test set-up and measurement system

Figure 1 a) shows for the rated motor power of 1.5 kW the three investigated four-pole ($2p = 4$) induction machines with a squirrel cage rotor. Figure 3 shows one of the investigated four-pole induction machines with rated power of 11 kW with its additional rotor imbalance. The machine stator windings are fed by IGBT-two-level-voltage source inverters with $U_d = 560$ V DC link voltage, type FC-302, Company *Danfoss*. At all measurements the switching frequency of the inverters is kept constant at 10 kHz. The induction machines are modified for bearing current measurements by insulated bearing seats. This bearing seat insulation is bridged by a short copper cable to measure the by-passing bearing currents as i_m (Fig. 7) via a current probe, IWATSU SS-250, instead of the real bearing current i_b. The schematic cross section of the machine in Figure 1 b) exhibits also the sliding carbon brush contact to measure the bearing voltage drop u_b.

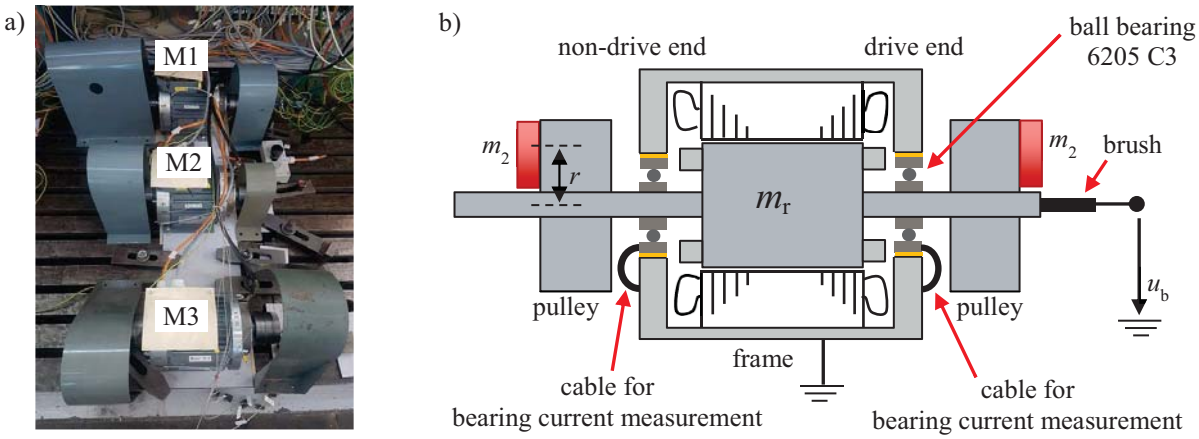

Fig. 1: a) Three TEFC standard cage induction machines M1, M2, M3 with rated power 1.5 kW at 400 V AC, are fed by three IGBT-two-level-voltage source inverters with $U_d = 560$ V DC link voltage, type FC-302, Company *Danfoss*. b) Schematic cross section of one cage induction machine (m_r: rotor mass) with an additional imbalance rotor mass m_2, mounted on the pulley at the drive end and non-drive end side. Both ball bearings, type 6205 C3, are electrically insulated towards the bearing seat. This bearing seat insulation is bridged via a short copper cable to measure the by-passing bearing currents via a current probe.

The motors were equipped at NDE and DE on the shaft with pulleys to increase the radial forces via the belt tension. Here the belt is removed to study only the influence of radial bearing forces, caused by rotor mass gravity, by the single sided magnetic pull due to a parasitic rotor eccentricity and by the rotor static imbalance forces. Figure 2 shows one of the three test motors of the test bench (Fig. 1 a) with a rated power of 1.5 kW with additional rotor masses attached on both pulleys (with removed belt) on drive end and non-drive end side, pointing in the same radial direction to cause an additional static rotor imbalance. Without the masses only the natural individual rotor imbalance U0 is present. With two different masses, equal at NDE and DE, two different bigger imbalances U1 and U2 are created. The imbalance U1 is simply realized by the cylindrical mass m at the radial distance r of the rotor shaft center (Fig. 2b), yielding $\Delta U1 = 2 \cdot m \cdot r$, with masses m on both NDE and DE. With (1) the additional imbalance $\Delta U2$ of the two semicircular "U-shaped" masses (Fig. 2 c) is calculated by inner and outer radii r_1 and r_2 as well as the axial length l and the mass density γ of steel with 7.9 g/cm³. The fixing screw is assumed to fill completely the drilled hole.

$$\Delta U2 = \frac{2}{3} \cdot l \cdot \gamma \cdot (r_2^3 - r_1^3) \cdot 2 \tag{1}$$

The resulting radial bearing force F_r consists of the rotor gravity force $F_g = m_r \cdot g$, the force $F_U = U \cdot (2\pi \cdot n)^2$ caused by static rotor imbalance and the inevitable single-sided magnetic pull F_m of the induction motor. With horizontal shaft, the rotor gravity force F_g acts at all time vertically downwards. The static rotor imbalance F_U rotates with the rotor speed n. The single-sided magnetic pull F_m acts in the direction of the smallest air gap δ at an assumed residual rotor eccentricity [1], which is at least one half of the radial internal bearing clearance of e.g. $P_d/2 = 10.25$ µm at the ball bearing type 6205 C3.
The single-sided magnetic pull F_m is calculated in Table I by (2), [1], considering the stator inner diameter d_{si}, the axial iron core length l_{Fe}, the radial flux density amplitude in the air gap $\hat{B}_{\delta s1} = 1$ T and the relative eccentricity ε, which is the eccentricity e related to the radial air gap width δ according to (3). The value $e = P_d/2$, but might be increased by a) static and b) dynamic rotor eccentricity due to a) manufacturing influence and b) due to rotor shaft bending [1]. Here is $e = P_d/2$, $\varepsilon = 4\%$.

$$F_m = \frac{\pi}{4 \cdot \mu_0} \cdot d_{si} \cdot l_{Fe} \cdot \varepsilon \cdot \hat{B}_{\delta s1}^2 \qquad 2p \geq 4 \tag{2}$$

$$\varepsilon = \frac{e}{\delta} \tag{3}$$

Table I gives an overview of the calculated mechanical and magnetic forces F_g, F_U and F_m at the two test benches with the 1.5 kW- and 11 kW-induction motors, where $e = P_d/2$ is assumed. The static rotor imbalance force is calculated with the highest investigated imbalance level ΔU2 at a rotor speed of 1000 min^{-1}.

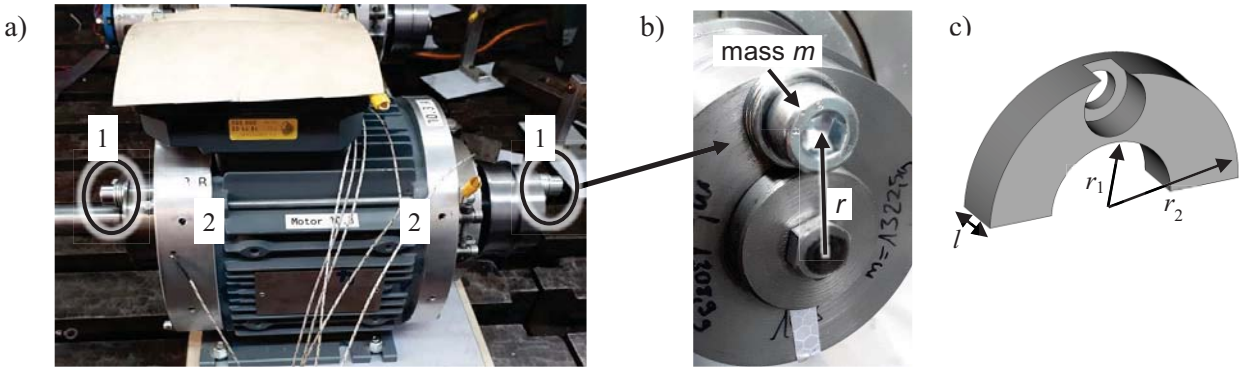

Fig. 2: a) Four-pole squirrel cage induction machine 1.5 kW, 400 V Y, prepared for bearing current measurements, with the additional static rotor imbalance ΔU1 (1), according to Fig. 2 b). At both bearing end shields are mounting holes (2) in radial direction for the fixation of the vibration sensor.
b) Static rotor imbalance ΔU1 = 1500 g·mm by the two additional masses m, here shown at the drive end side of the machine, at a distance r from the center of the rotor shaft. c) Sketch of one of the two additional "U-shaped" masses for the increased static rotor imbalance ΔU2 = 6264 g·mm.

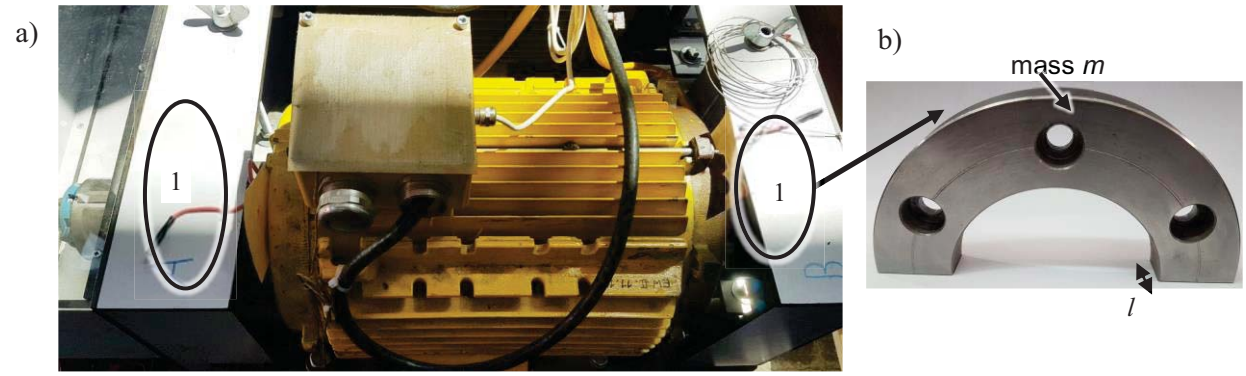

Fig. 3: a) One of the three four-pole TEFC squirrel cage standard induction machines with the rated power of 11 kW, prepared for bearing current measurements, with an additional static rotor imbalance ΔU2 (1). b) Additional "U-shaped" mass m to increase the static rotor imbalance to ΔU2 = 40031 g·mm at the drive end and non-drive end side of the machine.

Table I: Calculated rotor gravity forces, static rotor imbalance forces and magnetic forces of the two investigated induction machine power levels

P_N / kW	m_r / kg	F_g / N	ΔU2 / (g·mm)	ΔF_{U2} / N (n = 1000 min^{-1})	F_m / N
1.5	7.5	74	6264	68.7	99.9
11	39.6	388	40031	439.0	241.0

The residual imbalance due to the rotor manufacturing process could be measured on the balancing rotor test bench. Here for simplicity it was assumed that the maximum residual imbalance G6.3 according to DIN ISO 1940 Part 1 occurred at rated speed n_N = 1500 min^{-1}. The corresponding residual distance e_S of the rotor center of gravity from the rotor rotational axis is $e_S = G/(2\pi \cdot n_N)$. Hence the residual rotor imbalance force is $F_{U,res} = m_r \cdot e_S \cdot (2\pi \cdot n)^2$ at the rotor speed n, yielding $U0 = m_r \cdot e_S$. The resulting increased rotor imbalances are U1 = ΔU1 + U0 and U2 = ΔU2 + U0.
Figure 4 shows the calculated orbit of the resulting radial bearing force F_r during motor operation at the investigated 1.5 kW-induction machines at a rotor speed of n = 1000 min^{-1} with residual imbalance (Fig 4. a) and increased imbalance (Fig 4. b), always with additional single sided magnetic pull F_m. Only between three and five of the nine balls of the bearing 6205 C3 are radially loaded during motor operation at the lower half of the bearing, labeled as bearing load zone.
If the rotor speed n rises strongly or the static rotor imbalance U increases, the resulting radial bearing force is increased in that way, that the bearing load zone rotates in the bearing at the whole bearing circumference raceway.

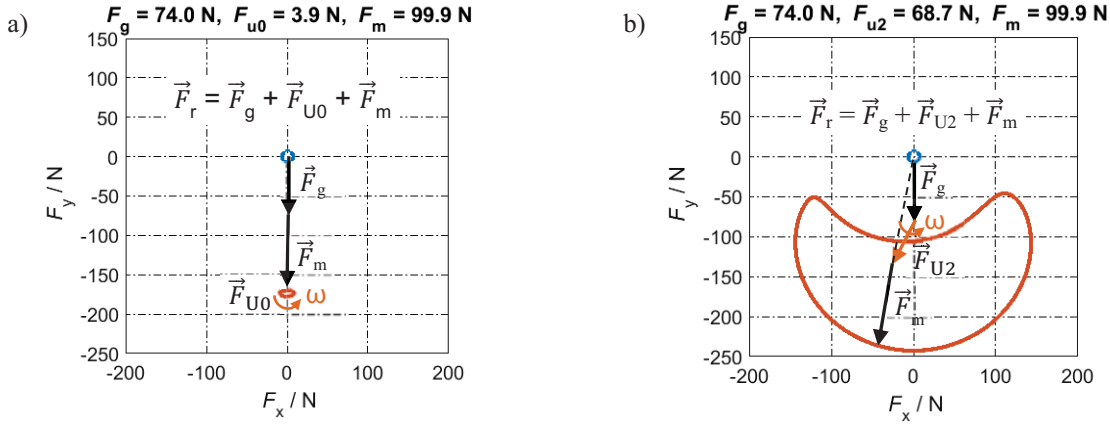

Fig. 4: Calculated orbit of the radial bearing force vector $\vec{F}_r$ during motor operation of the 1.5 kW-induction machine at a rotor speed n = 1000 min^{-1} ($\omega = 2\pi \cdot n$). The single-sided magnetic pull F_m acts in direction of the smallest air gap.
a) Considering rotor mass gravity force F_g, magnetic pull F_m and rotational force due to residual imbalance $F_{U,res} = F_{U0}$.
b) Like a), but with increased static rotor imbalance force F_{U2}.

Bearing Current Measurements with static rotor imbalance

EDM bearing currents at 1.5 kW-induction motor

Figure 5 shows the measured peak-to-peak EDM bearing current amplitudes immediately after lubrication film breakdown of induction motor M3 (rated power 1.5 kW) at three different static rotor imbalances U0, U1, U2 (Table II). The shown values are the average of 50 EDM events (z) along with the 1σ-deviation band ($z \pm \sigma$), measured in steps of Δn = 150 min^{-1}. In case of Fig. 5 c) without additional static rotor imbalance only the residual imbalance U0 is active. Here the EDM bearing currents occur in a speed range of 300 … 1900 min^{-1} with an average bearing current peak-to-peak value of $I_{m,av}$ = 0.65 A. Below 300 min^{-1} the lubrication film is too thin, so metallic contact may occur,

prohibiting a film breakdown. Above 1900 min^{-1} the film thickness is big enough, so the electric field strength $E_b = \hat{U}_b/h$ is smaller than the breakdown field strength E_D. The voltage $\hat{U}_b$ is the bearing voltage shortly before the EDM breakdown occurs (Fig. 5d). The higher the rotor imbalance is, the smaller is the rotor speed range, where EDM bearing currents occur as well as the higher is the average bearing current peak-to-peak value up to $I_{m,av}$ = 1.10 A. In the grey marked rotor speed range, there was no measurement possible due to high mechanical motor vibrations, caused by the additional rotor imbalance. An explanation for the reduced speed range of EDM currents at higher imbalance is missing until now. Obviously the lubrication film thickness is increased.

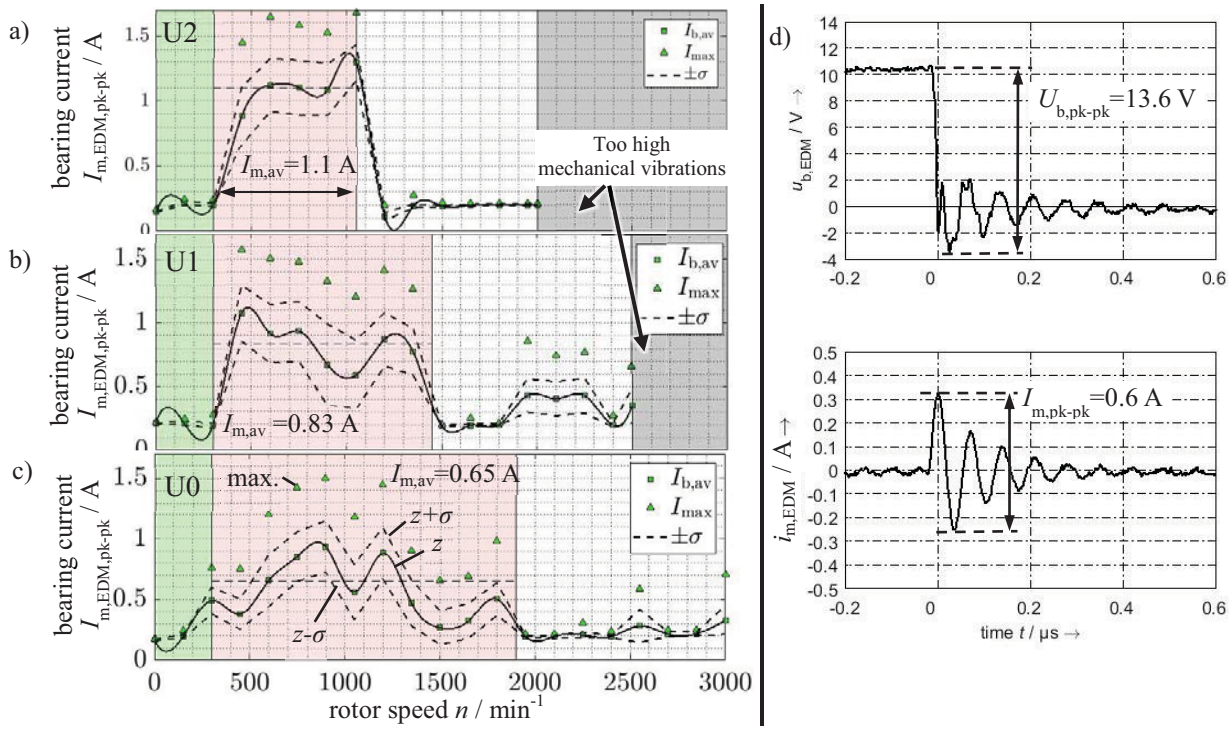

Fig. 5: Measured peak-to-peak values of EDM bearing currents over rotor speed (0 … 3000 min^{-1}) at NDE side of inverter-fed motor M3 for a) a high static rotor imbalance U2, b) small static rotor imbalance U1, and c) with residual rotor imbalance U0 due to manufacturing process. d) Measured typical EDM bearing voltage and current at NDE side of the inverter-fed motor M3 at rotor speed n = 750 min^{-1} and with rotor imbalance U0.

Rotor-to-ground bearing currents at 1.5 kW-induction motor

The rotor of the 1.5 kW-test motor M3 (Fig. 1a) is grounded via a rotor-sliding carbon brush connected to a grounding cable. To force the bearing current through the test bearing at the DE side, the NDE side bearing is electrically insulated towards the bearing end shield. The resulting equivalent capacitive circuit of the electric machine is shown in Fig. 7. Figure 6 shows the measured peak-to-peak rotor-to-ground bearing currents $I_{m,DE}$ of the 1.5 kW-induction motor M3 at the three different static rotor imbalances U0, U1, U2 (Table II). The rotor-to-ground bearing current i_b occurs at each change of the inverter output common-mode voltage u_{CM} as a common-mode effect and is limited by the impedance of the whole grounding path from stator winding potential to ground potential. So the influence of the bearing impedance is only a small part of that impedance and is due to $R_{b,DE} \gg 1/(\omega_{HF} \cdot C_{b,DE})$ mainly an ohmic bearing current. This current is obviously only slightly increasing with speed and with imbalance, so it is mainly independent of additional rotor imbalance forces. The i_m-occurrence rate is 6·10 kHz = 60 kHz.

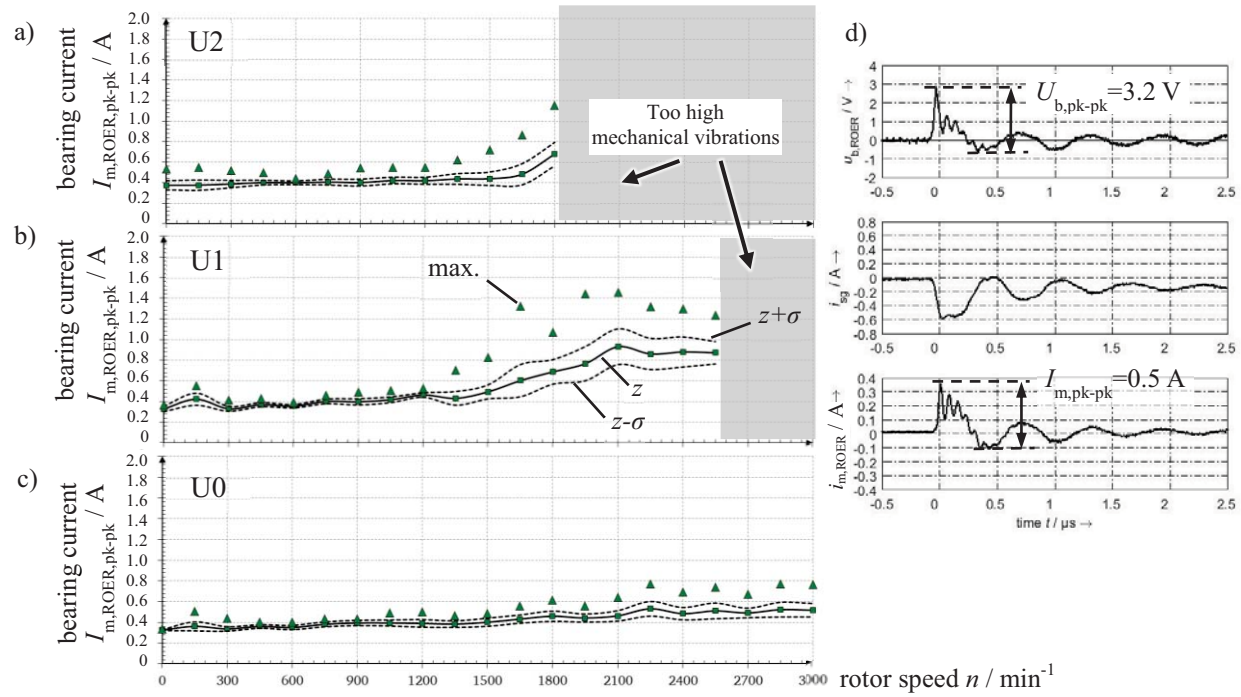

Fig. 6: Like Fig. 5, but with rotor-to-ground bearing currents i_{rg} (abbreviation: ROER) via the rotor grounding. The average of 50 current events (z) is shown along with the 1σ-deviation and the maximum amplitude (max.) out of 50 events. d) Measured typical rotor-to-ground bearing voltage, stator-to-ground current i_{sg} and bearing current at DE side of inverter-fed 1.5 kW motor M3 at rotor speed n = 1500 min^{-1} and with rotor imbalance U1.

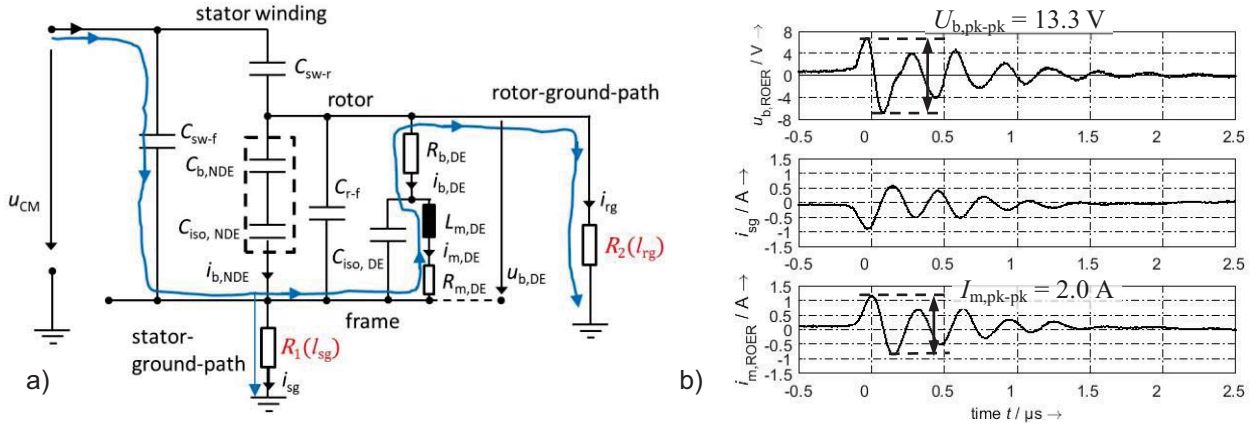

Fig. 7: a) Equivalent capacitive circuit for cage induction-motor without considering the stator winding inductance, for HF AC common-mode currents and a rotor-to-ground bearing current i_{rg}. The test bearing is at DE. The NDE bearing is electrically insulated towards the bearing end shield.
b) Measured typical rotor-to-ground bearing voltage, stator-to-ground current i_{sg} and bearing current at DE side of inverter-fed 11 kW-induction motor of long-term test of Fig. 13 a) at 1022 h.

Table II: Calculated static rotor imbalances of the two investigated induction machines

P_N / kW	Maximum permissible residual imbalance U0 at balance quality G6.3 / (g·mm)	ΔU1 / (g·mm)	ΔU2 / (g·mm)
1.5	352	1498	6322
11	1702	not tested	40379

Long-term test with EDM and rotor-to-ground bearing currents at 1.5 kW-induction motor

The change in the bearing raceway surface is analyzed after 1000 h-long-term tests with EDM (Fig. 8) and rotor-to-ground bearing currents (Fig. 9) at increased imbalances ΔU1 and ΔU2. In case of EDM

bearing currents and a static rotor imbalance ΔU1 only a grey racetrack surface (grey "frosting") at the bearing surface was detected after 1000 h of operation, as the EDM bearing currents occur only with roughly 1/1000 of the rotor-to-ground occurrence rate. So the craters on the racetrack due to sparking are smoothened by the by-passing roller elements between two EDM current events.
With rotor-to-ground bearing currents and a static rotor imbalance U2 the bearing raceway surface of the lower half of the outer bearing ring shows fluting after 1000 h of operation, with the bearing current amplitude is much smaller than with EDM currents. Due to the 60 kHz-occurrence rate there is no time for smoothing the raceway by the roller elements between two bearing current events. So the fluting process may be started.

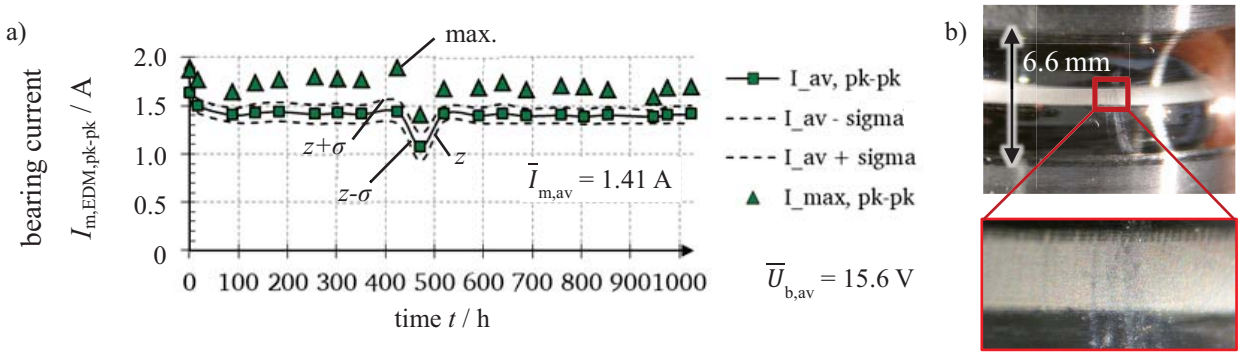

Fig. 8 a) Static rotor imbalance ΔU1: Measured peak-to-peak values of EDM bearing currents at the 1.5 kW-induction motor M3 at NDE side during operating time of 1024 h at rotor speed n = 1000 min^{-1} and average bearing temperature ϑ_b = 50 °C.
b) Grey racetrack on outer bearing raceway after 1024 hours of operation.

With an average bearing current peak-to-peak value of $I_{m,pk-pk}$ = 0.37 A and an analytically calculated *Hertz*'ian area of A_{Hertz} = 0.434 mm², the apparent bearing current density [3] is calculated for rotor-to-ground bearing currents as $J_b \approx (2/3) \cdot I_{m,pk-pk}/A_{Hertz}$ = 0.57 A/mm², but $J_b \approx$ 2.17 A/mm² for EDM currents. With an apparent bearing current density limit of 0.1 A/mm² for DC and low frequency AC bearing currents, due to 0.57 A/mm² > 0.1 A/mm² fluting is predicted [3]. The 1/1000-times lower occurrence rate of EDM bearing currents allows the surface smoothening effect, so the much higher value $J_b \approx$ 2.17 A/mm² > 0.1 A/mm² does not lead to fluting.

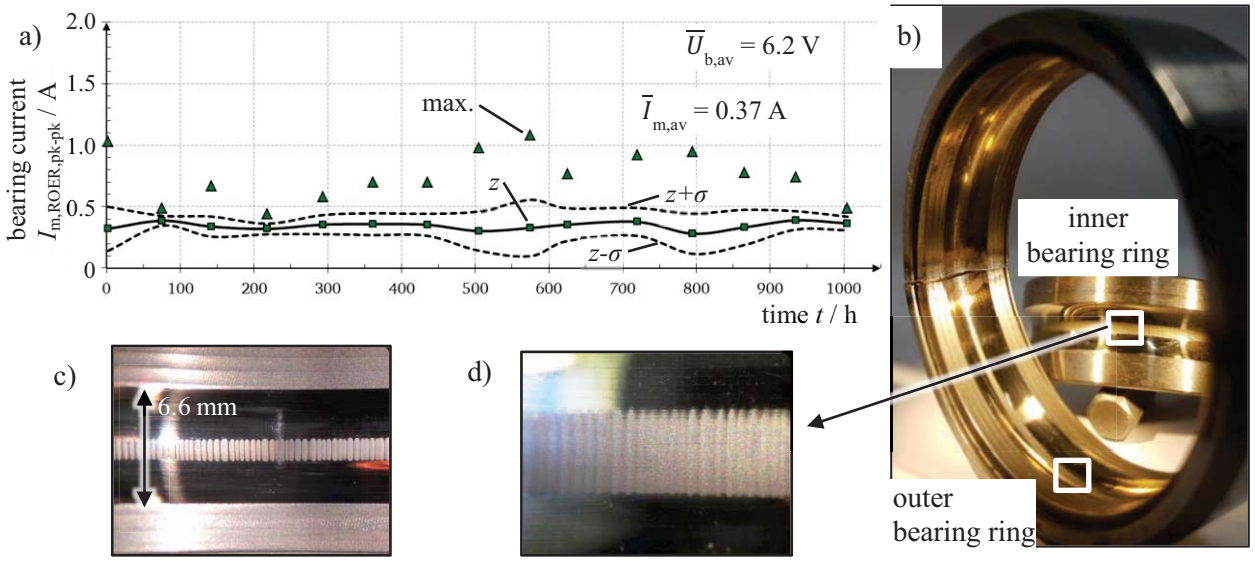

Fig. 9 a) Static rotor imbalance ΔU2: Measured peak-to-peak values of rotor-to-ground bearing currents at 1.5 kW-induction motor M3 at DE side during operating time of 1024 h at a rotor speed n = 1000 min^{-1} and at an average bearing temperature ϑ_b = 50 °C.
b) Damaged bearing with fluting at the racetrack surface of the lower half part (load zone) of the outer bearing ring, type 6205 C3.
c) Fluting at the surface only in the load zone of the outer bearing ring.
d) Fluting at the whole surface of the inner bearing ring, due to continuous ring rotation.

Figure 10 shows the measured mechanical radial acceleration at the DE side of the bearing end shield versus frequency during the operating time *t*. The mechanical acceleration at the characteristic frequency of 2.4 kHz exceeds at 700 h the limit of 2 m/s² for safe bearings, according to [9]. The fluting effect for rotor-to-ground bearing currents was not accelerated by increased imbalances ΔU1, ΔU2 in comparison to U0, whereas with EDM bearing currents no fluting occurred, independent of U0, ΔU1, ΔU2.

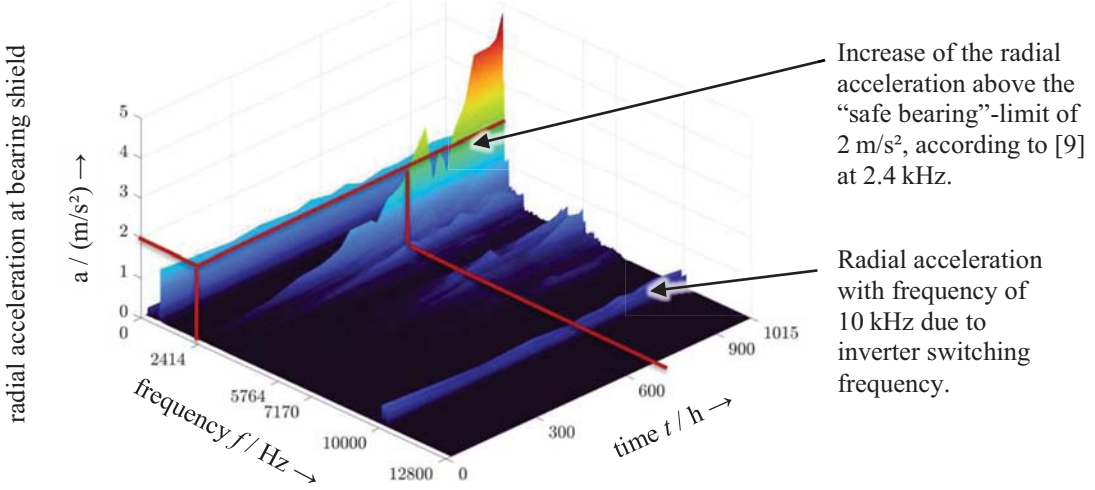

Fig. 10 a) Effect of the static rotor imbalance ΔU2: Measured radial mechanical acceleration (rms-value) with *Smart Balance 2* from Company *Schenck* at the DE bearing end shield of the 1.5 kW-induction motor M3 during operating time of 1024 h. Test with rotor-to-ground bearing currents, rotor speed $n = 1000\ \text{min}^{-1}$, average bearing temperature $\vartheta_b = 50\ °C$, inverter switching frequency $f_{IGBT} = 10$ kHz.

Long-term test with EDM and rotor-to-ground bearing currents with 11 kW-induction motors

The three investigated four-pole 11 kW-induction machines (Fig. 3) were operated in parallel for 1040 hours with increased static rotor imbalance ΔU2 (Table II) with the occurrence of EDM bearing currents, caused by the sparking of the lubrication film due to the common-mode bearing voltage exceeding frequently the discharge threshold. The measured peak-to-peak EDM bearing currents at the DE side of the 11 kW-induction motor M1 in dependence of the operating time are shown in Fig. 11.

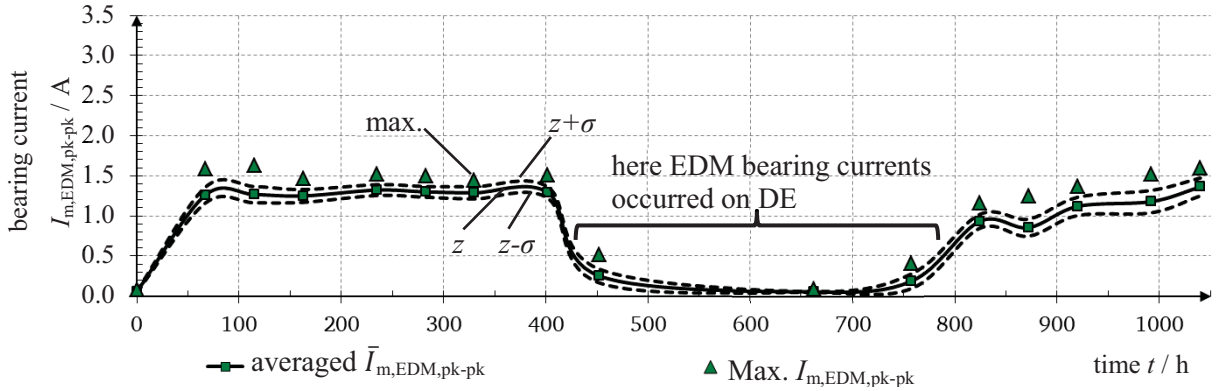

Fig. 11: Static rotor imbalance ΔU2: Measured peak-to-peak EDM bearing currents at the 11 kW-induction motor M1 at NDE side during operating time of 1040 h at rotor speed $n = 1000\ \text{min}^{-1}$ and average bearing temperature $\vartheta_b = 60\ °C$.

EDM bearing currents occurred, which are statistically distributed between the bearing DE and NDE side. Table III shows the results of the long-term test with all three 11 kW-induction machines. The maximum apparent bearing current density occurs with 0.41 A/mm² at non-drive end side of motor M2. A grey raceway (Fig. 12a) occur on the investigated ball bearings, although the maximum apparent bearing current density was rather big 0.41 A/mm² > 0.1 A/mm², due to the low occurrence

rate of EDM events. If $J_b < 0.1$ A/mm², even no "grey frosting" occurs, but the raceway surface is unchanged Fig. 12b).

a)  b) 

Fig. 12: According to Fig. 11: a) Inner bearing ring racetrack of the DE side bearing with a grey raceway. b) Inner bearing ring racetrack of the NDE side, showing no change of raceway surface.

Table III: Static rotor imbalance ΔU2, 1000 min^{-1}, measured EDM bearing currents: Long-term test with three 11 kW-induction machines M1, M2, M3.

Drive end side	motor M1	motor M2	motor M3
av. bearing voltage $U_{b,av}$	10.66 V	12.46 V	8.47 V
confidence interval $\sigma_{u,av}$	1.23 V	1.27 V	1.48 V
av. bearing current $I_{m,EDM,pk\text{-}pk,av}$	0.94 A	0.12 A	0.47 A
confidence interval $\sigma_{i,av}$	0.08 A	0.01 A	0.08 A
apparent bearing current density J_b	**0.39 A/mm²** > 0.1	**0.05 A/mm²** < 0.1	**0.20 A/mm²** > 0.1
bearing surface of inner ring	grey raceway	no surface change	grey raceway
Non-drive end side			
av. bearing voltage $U_{b,av}$	10.56 V	13.44 V	4.46 V
confidence interval $\sigma_{u,av}$	1.34 V	1.27 V	1.18 V
av. bearing current $I_{m,EDM,pk\text{-}pk,av}$	0.08 A	0.98 A	0.05 A
confidence interval $\sigma_{i,av}$	0.01 A	0.09 A	0.01 A
apparent bearing current density J_b	**0.03 A/mm²** < 0.1	**0.41 A/mm²** > 0.1	**0.02 A/mm²** < 0.1
bearing surface of inner ring	no surface change	grey raceway	no surface change

In comparison with the same tests at residual static imbalance U0, no influence of the increased rotor imbalance ΔU2 on the bearing surface was detected. Similar to the long-term test of Fig. 11, a long-term test with rotor-to-ground bearing currents was investigated with the static rotor imbalance ΔU2 (Fig. 13). The three investigated four-pole 11 kW-induction machines (Fig. 3) were operated over 1023 hours with static rotor imbalance ΔU2 and rotor-to-ground bearing currents at DE side. The measured rotor-to-ground bearing currents at DE side of 11 kW-induction motor M1 over operating time are shown in Fig. 13. Table IV summarizes the results of the long-term test with rotor-to-ground bearing currents at 11 kW-induction machines over 1023 hours. Again no influence of the increased static rotor imbalance ΔU2 on the bearing raceway damage was found.

In a similar way to Fig. 13, a long-term test with 11 kW-induction machines was performed at imbalance ΔU2, but at grid operation 50 Hz, 400 V, n = 1500 min^{-1}. No bearing currents occurred during operating time of 1031 h, and no change of the raceway surfaces of the bearings were detected.

Table IV: Static rotor imbalance ΔU2, 1000 min^{-1}, measured rotor-to-ground bearing currents: Long-term test at three 11 kW-induction machines M1, M2, M3.

Drive end side	motor M1	motor M2	motor M3
av. bearing voltage $U_{b,av}$	14.30 V	16.78 V	12.56 V
confidence interval $\sigma_{u,av}$	1.31 V	0.98 V	0.73 V
av. bearing current $I_{m,ROER,pk\text{-}to\text{-}pk,av}$	2.13 A	5.50 A	5.08 A
confidence interval $\sigma_{i,av}$	0.18 A	0.27 A	0.18 A
apparent bearing current density J_b	**0.89 A/mm^2** > 0.1	**2.29 A/mm^2** > 0.1	**2.12 A/mm^2** > 0.1
bearing surface of inner ring	grey raceway	starting fluting	starting fluting

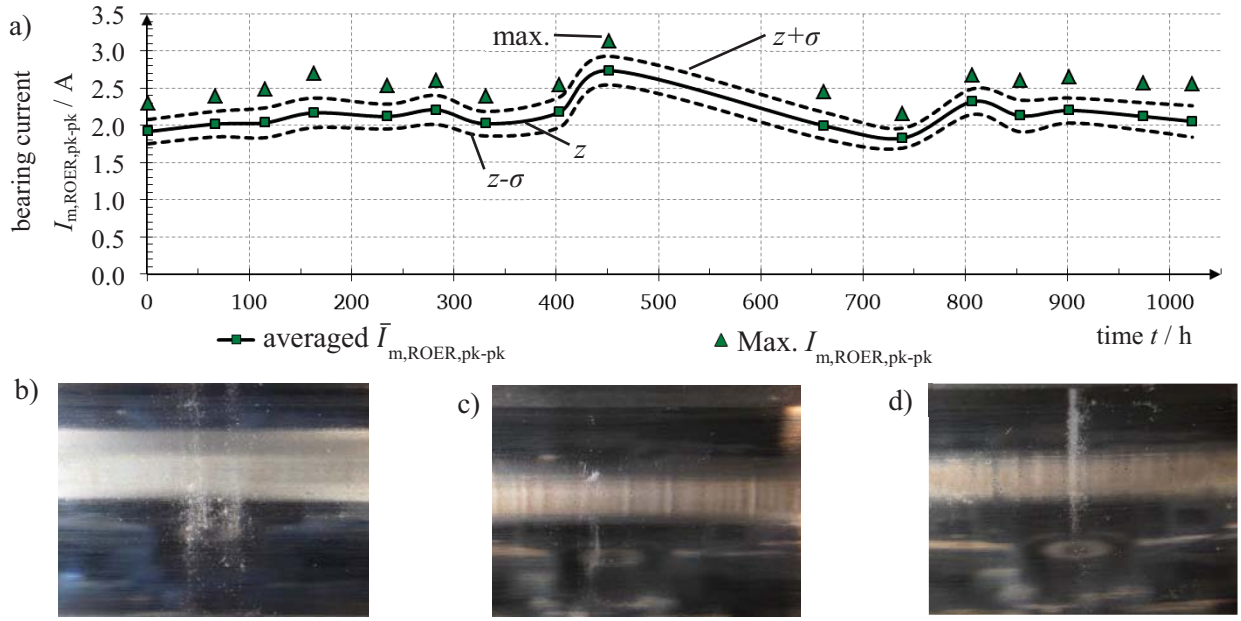

Fig. 13 a) Static rotor imbalance ΔU2: Measured peak-to-peak rotor-to-ground bearing currents at the 11 kW-induction motor M1 at the DE side during an operating time of 1023 h at a rotor speed n = 1000 min^{-1} and an average bearing temperature ϑ_b = 60 °C.
b) Inner bearing ring of the DE side bearing of motor M1 with a grey raceway.
c) Inner bearing ring of the DE side bearing of motor M2 with beginning of fluting.
d) Inner bearing ring of the DE side bearing of motor M3 with beginning of fluting.

Conclusion

With three 1.5 kW- and three 11 kW-4-pole cage induction standard TEFC motors (frame sizes 90 mm and 160 mm) short-term and 1000 h long-term tests were performed to find out, whether an additional static rotor imbalance accelerates the bearing damage under an inverter-induced bearing current flow. Two types of inverter-induced bearing currents were investigated: EDM bearing currents due to electrical lubrication film breakdown, caused by the common-mode bearing voltage, and the common-mode rotor-to-ground bearing currents in case of grounded rotor, e.g. via a gear or conductive belt. The latter have the same occurrence rate of 6-times inverter switching frequency and a similar time signal shape as the circular inverter-induced bearing currents, which occur in bigger AC machines typically above frame size 200 mm [3]. The static rotor imbalance was enlarged by additional rotor masses by a factor of 4 and 16 as ΔU1 and ΔU2 for the 1.5 kW-induction motors with respect to the residual imbalance limit U0 according to G6.3 of DIN ISO 1940 Part 1. For the 11 kW-induction motors the imbalance was enlarged with ΔU2 by a factor 16. The occurring n-frequent vertical and

horizontal bearing vibration could accelerate the bearing fluting damage, which is believed according to [5] to be generated by bearing vibrations, caused by the small bearing surface craters of the sparking bearing current flow. Although these additional vibrations occurred, these additional imbalances have no influence on an accelerated electrical bearing current damage. The EDM bearing currents have, like without additional rotor imbalance, a roughly 1000-times smaller occurrence rate than the rotor-to-ground bearing currents, which flow at each inverter-switching instant, thus with 6-times the switching frequency, so here 60 kHz. Hence, the well-known limit of 0.1 A/mm² of apparent bearing current density to avoid fluting, which was derived from DC and LF AC bearing currents, did only apply to the rotor-to-ground bearing currents. For EDM currents even apparent bearing current densities up to 2 A/mm² did not cause any fluting, but resulted only in a "grey frosted" bearing racetrack, which still allows stable operation, so the influence of increased static rotor imbalance on the electric bearing damage may be disregarded at least within the scope of the presented experimental data, whereas the type of bearing current, either EDM or rotor-to-ground bearing currents is decisive for the electrical bearing damage.

References

[1] Werner U., Binder A.: "Rotor dynamic analysis of asynchronous machines including the finite-element-method for engineering low vibration motors," *Proc. of international Symposium on Power Electronics, Electrical Drives, Automation and Motion* (SPEEDAM), 23. - 26.05.2006, Taormina, Italy, pp. 88-96.

[2] Sunahara K. et al., "Effect of lubrication regime on washboard/fluting pattern formation due to electrical pitting", poster presentation at 43rd Leeds-Lyon Symposium on Tribology, 2016.

[3] Muetze A., Binder A., Vogel H., Hering J., "Experimental evaluation of the endangerment of ball bearings due to inverter-induced bearing currents," *Proc. of the 2004 IEEE Industry Applications Conf.*, Seattle, WA, USA, 03. - 07. October, 2004, vol. 3, pp. 1989 - 1995.

[4] Binder A., Muetze A., "Scaling effects of inverter-induced bearing currents in AC machines," *IEEE Transactions on Industry Applications*, vol. 44, no. 3, pp. 769 - 776, June 2008.

[5] Kohaut A.: "Riffelbildung in Wälzlagern infolge elektrischer Korrosion, (English: Fluting in bearings due to electrical corrosion)," Julius-Maximilians-Universität, Würzburg, Germany, habilitation thesis, 1943.

[6] Wittek E., Kriese M., Tischmacher H., Gattermann S., Ponick B., Poll G., "Capacitances and lubricant film thicknesses of motor bearings under different operating conditions," *Proc. of 2010 XIX International Conference on Electrical Machines*, 6 pages, CD ROM, Rome, Italy, 06. - 08. September, 2010.

[8] VDI-Guideline 3832, Measurement of structure-borne sound of rolling element bearings in machines and plants for evaluation of condition, April 2013, Düsseldorf, Germany.

[9] IEC 60034-14:2018, Rotating electrical machines - Part 14: Mechanical vibration of certain machines with shaft heights 56 mm and higher – Measurement, evaluation and limits of vibration severity (IEC 60034-14:2018), Geneva, Switzerland.

[10] DIN 620-4:2004-06, Rolling bearings - Rolling bearing tolerances - Part 4: Radial internal clearance (DIN 620-4:2004), Beuth, Berlin, Germany.